Supporting Information

FeO_x Nanoparticle Doping on Cu/Al_2O_3 Catalysts for the Reverse Water Gas Shift

*Ergys Pahija‡[1], Christopher Panaritis‡[1], Brian Rutherford[1], Martin Couillard[2], Bussaraporn Patarachao[2], Jalil Shadbahr[2], Farid Bensebaa[2], Gregory S. Patience[1] and Daria C. Boffito[1]**

Table S1 Conversion of CO_2 for different catalytic compositions and CO_2/H_2 ratios.

Catalyst	CO_2:H_2	CO_2 conversion	Reference
$10Cu/SiO_2$	1:1	8% (600 °C) → <1%	[1]
$0.3Fe/SiO_2$	1:1	1% (600 °C) → <1%	
$10Cu0.3Fe/SiO_2$	1:1	15% (600 °C) → 12% after 100h	
$15.1Fe/Al_2O_3$	1:4	22% (400 °C) 54% (600 °C)	[2]
$14.8Fe10.2Cu/Al_2O_3$	1:4	35% (400 °C) 58% (600 °C)	
$5Cu/CeO_2$	1:1	20% (600 °C)	[3]
$5Cu1.6Fe/CeO_2$	1:1	29% (600 °C)	[3]
$4Cu1Fe/Al_2O_3$	1:1	42% (700 °C)	[4]
$15.5Fe39.3Cu/CeO_2$	1:4	41% (400 °C) 65% (400 °C)	[5]
$10Cu5Fe/CeO_2$	1:1	25% (450 °C) 42% (650 °C)	[6]
$5Cu0.5Fe/SiO_2$	1:3	0% (300 °C) 35% (550 °C)	[7]

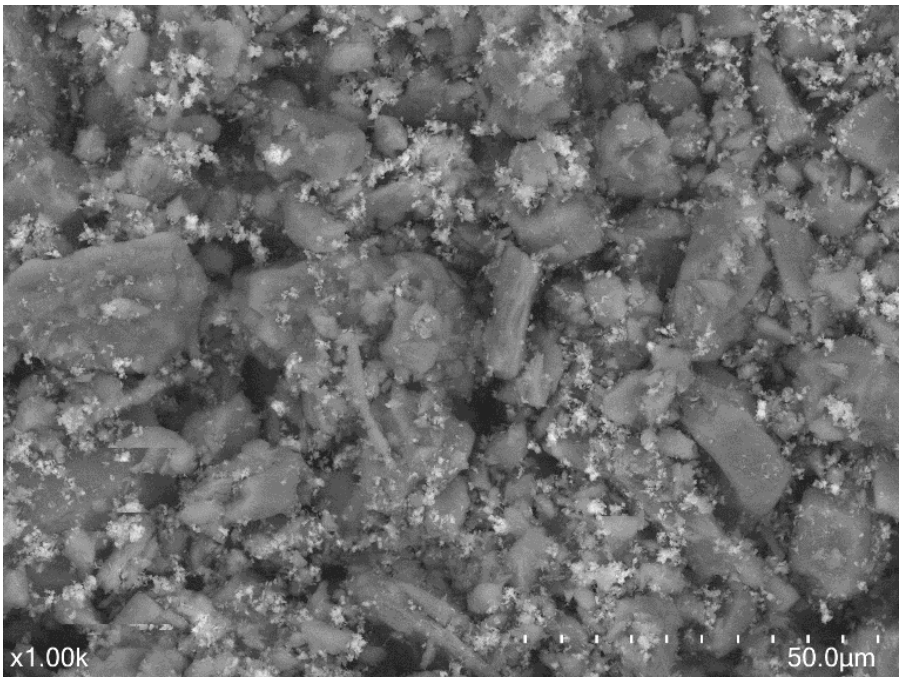

Figure S1 SEM image of CF09 catalyst. White flakes of CuO deposited on the Al2O3 support (gray area). Fe is indistinguishable in this image but detected by EDX (Fig. S2-S4).

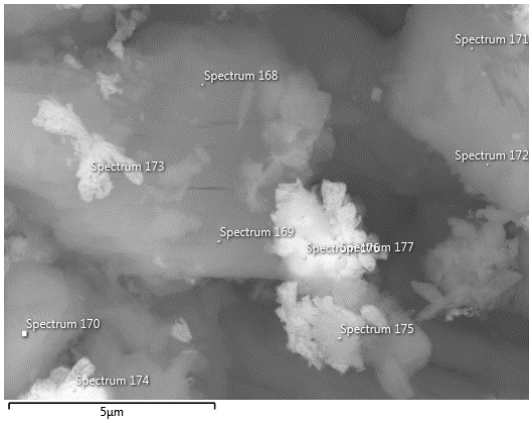

Spectra	C	O	Al	Fe	Cu
168	5.08	42.14	47.4	0.35	5.03
169	3.31	45.47	46.48	0.23	4.51
170	4.29	54.85	36.83	0.17	3.86
171	6.17	50.21	37.35	0.31	5.96
172	4.64	49.28	38.46	0.47	7.15
173	5.85	44.45	35.95	0.1	13.64
174	10.32	47.77	24.32	0.15	17.44
175	4.87	44.29	37.54	0.21	13.08
176	4.17	36.59	34.7	0.27	24.27
177	4.05	35.51	30.39	0.17	29.88
Max	10.32	54.85	47.4	0.47	29.88
Min	3.31	35.51	24.32	0.1	3.86
Average	5.275	45.056	36.942	0.243	12.482
Std Dev	1.964746	5.963983	6.761314	0.110156	9.02046

Figure S2. EDX analysis of CF03 and corresponding spectra compositions.

Spectra	C	O	Al	Fe	Cu
178	13.72	59.89	25.71	0.06	0.61
179	10.21	57.46	31.66	0.07	0.59
180	11.25	56.51	31.76	0.02	0.46
181	18.22	55.25	24.97	0.5	1.05
182	24.65	53.01	20.93	0.2	1.21

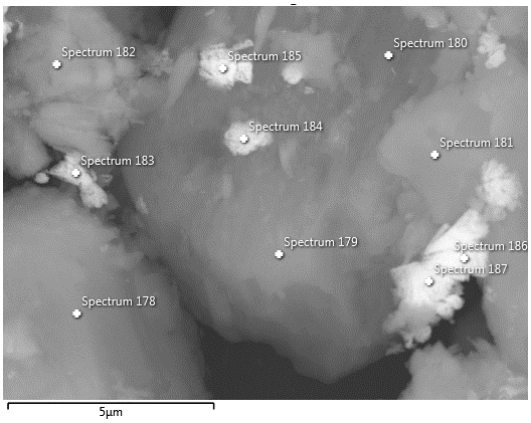

183	50.06	34.71	12.26	0.12	2.85
184	13.14	55.6	27.82	0.09	3.35
185	19.64	51.8	24.14	0.09	4.32
186	24.09	47.65	18.27	0.12	9.87
187	23.11	48.18	21.65	0.13	6.92
Max	50.06	59.89	31.76	0.5	9.87
Min	10.21	34.71	12.26	0.02	0.46
Average	20.81	52.01	23.92	0.14	3.12
Std Dev	11.582	7.222227	5.989892	0.135319	3.149565

Figure S3. EDX Analysis of CF06 and corresponding spectra compositions.

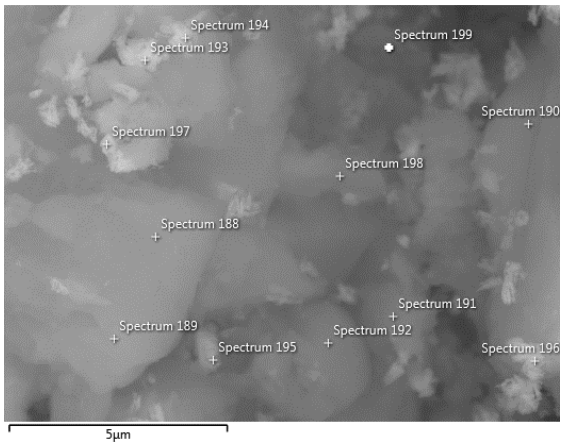

Spectra	C	O	Al	Fe	Cu
188	4.74	58.44	35.31	0.16	1.35
189	3.68	54.99	39.23	0.22	1.89
190	6.21	61.07	31.06	0.2	1.47
191	5.71	58.93	32.87	0.38	2.12
192	4.76	58.68	35.28	0.17	1.1
193	8.68	57.44	27.66	0.37	5.86
194	8.82	55.77	27.29	0.33	7.79
195	5.42	44.42	39.98	0.34	9.84
196	8.18	57.33	30.27	0.23	3.99
197	7.77	58.79	29.5	1.26	2.68
198	5.29	60.45	31.8	0.6	1.85
199	5.03	57.88	32.66	0.97	3.45
Max	8.82	61.07	39.98	1.26	9.84
Min	3.68	44.42	27.29	0.16	1.1
Average	6.190833	57.01583	32.7425	0.435833	3.615833
Std Dev	1.732058	4.318835	4.083568	0.345187	2.806578

Figure S4. EDX Analysis of CF09 and corresponding spectra compositions.

The dominating Cu plane measures 0.28 nm associated with CuO(001) [8 9]. The Cu-oxide phase is affiliated with the calcination treatment. The increase in Fe concentration translated into an increasing distance among planes, going from 0.28 nm in the CF03 sample to 1.16 nm [10] in the CF09 (Figure S5(c)). 0.278 nm corresponds to α-Fe_2O_4 (104) [11]. Liu et al. synthesized the catalyst through a sequential impregnation [11].

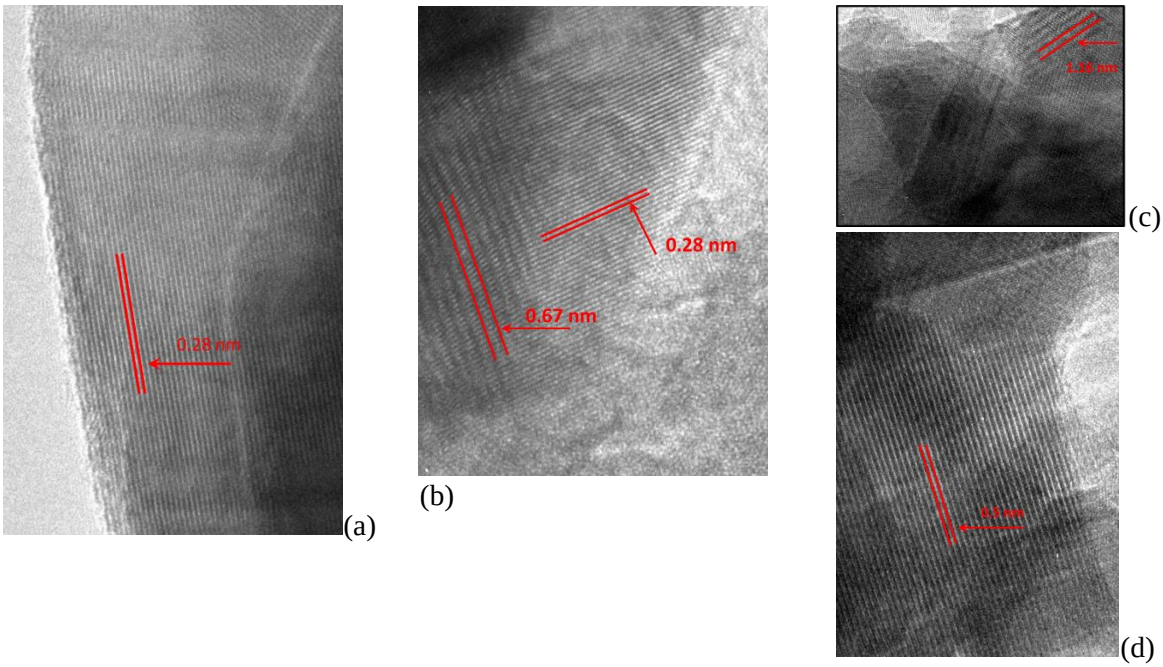

(a) (b) (c) (d)

Figure S5. TEM images from CF03 (a), CF06 (b) and CF09 (c) (d).

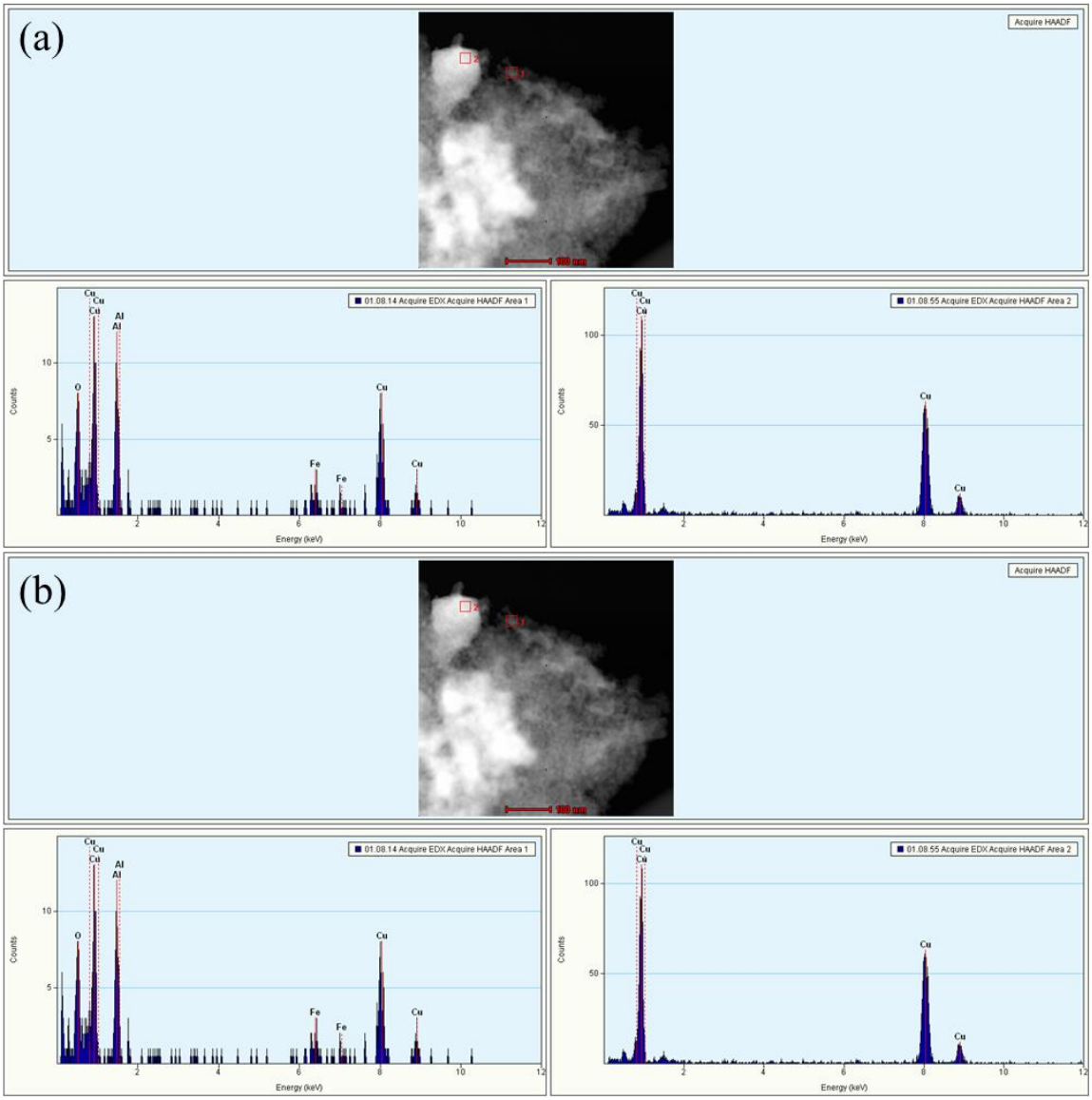

Figure S6. EDS Spectra of used (a) CF03 and (b) CFNP09. The brighter/whiter areas and gray area represent Cu and CuFe, respectively.

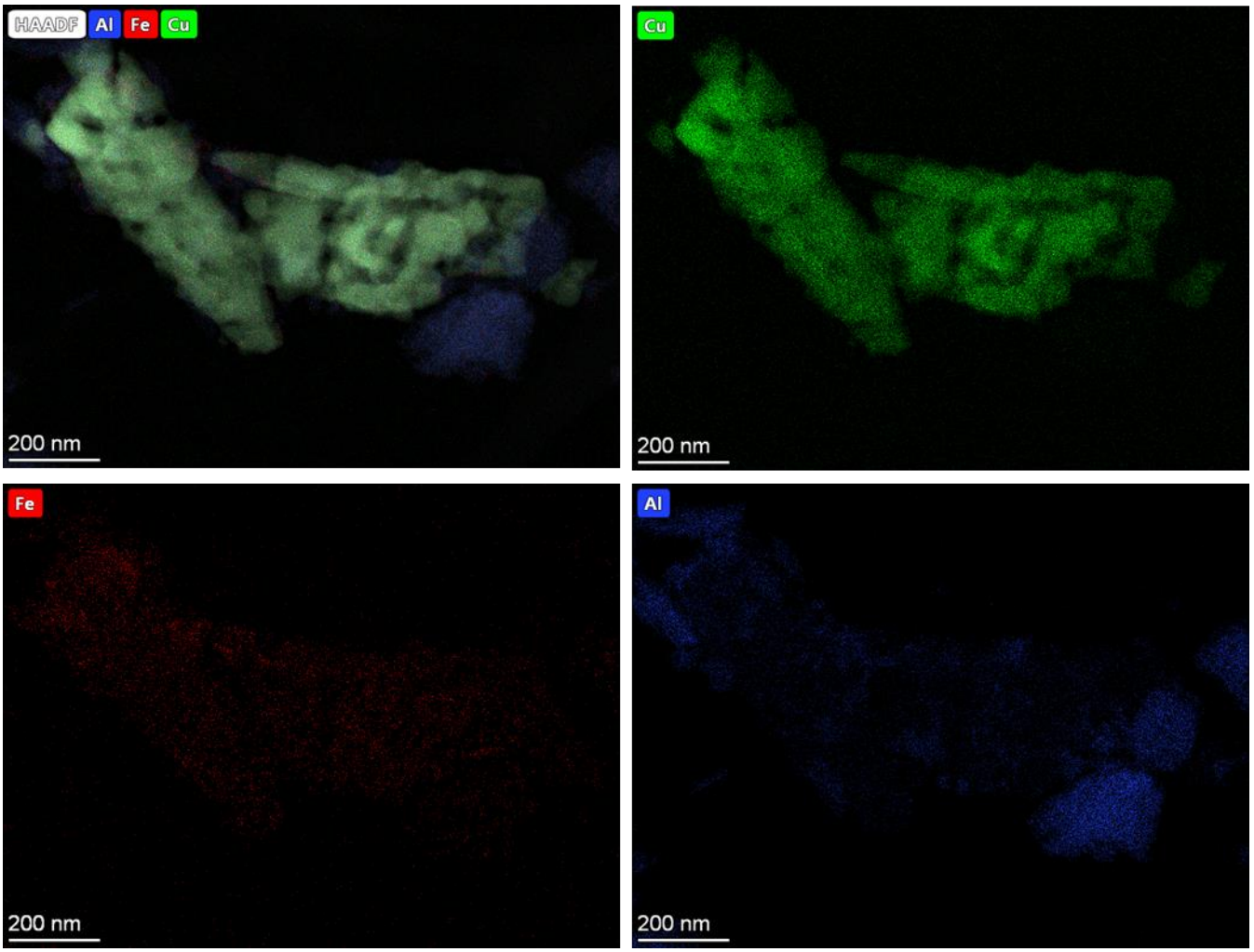

Figure S7. EDX of fresh CFNP09. Where Fe, Cu, and Al is depicted as red, green and blue, respectively.

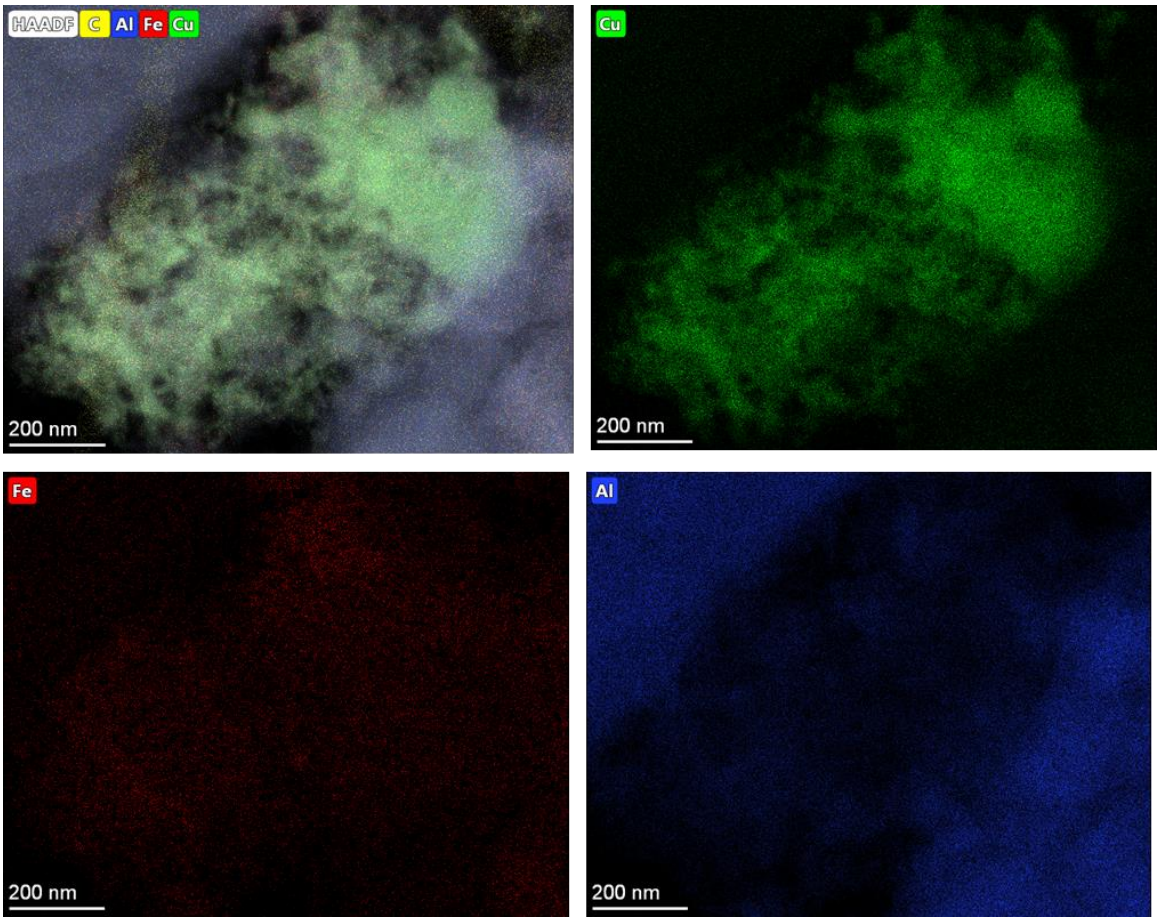

Figure S8. EDX image of used CFN09. Where Fe, Cu, Al, and C is depicted as red, green, blue, and yellow, respectively.

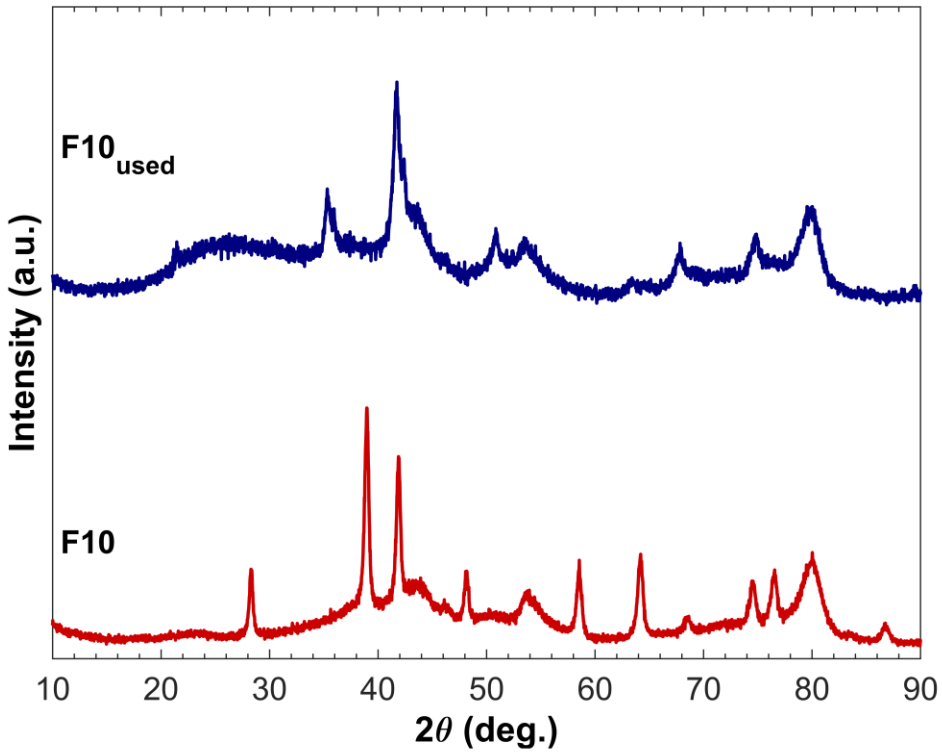

Figure S9. XRD patter of 10 Fe on Al_2O_3 (F10) and after activation/reaction ($F10_{used}$).

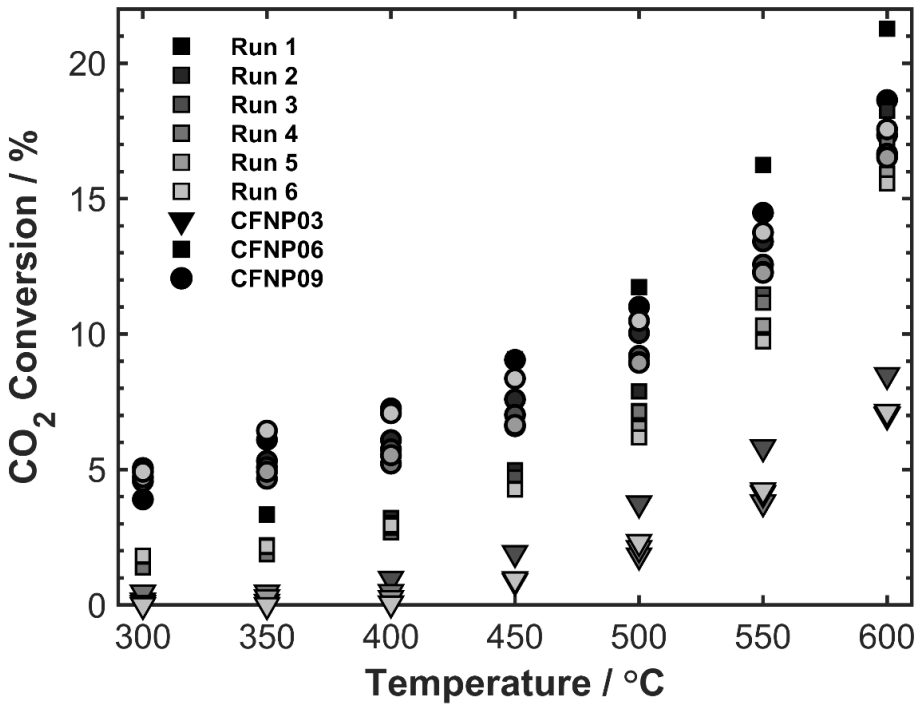

Figure S10. Catalytic activity and stability summary of catalysts: CFNP03, CFNP06, and CFNP09.

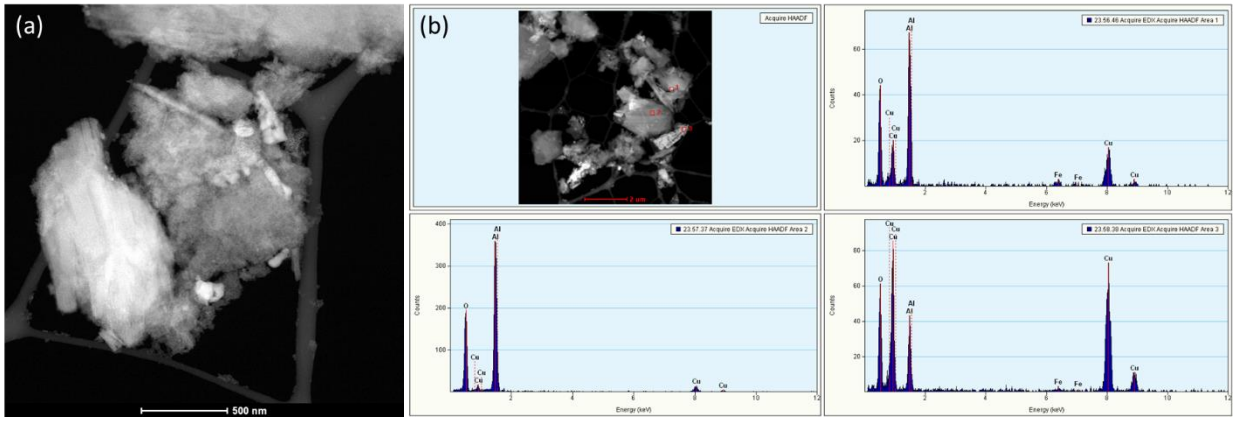

Figure S11. (a) STEM image and (b) EDX of fresh CFNP09. The bright white areas represent Cu and the lighter gray area represent a mix of CuFe.

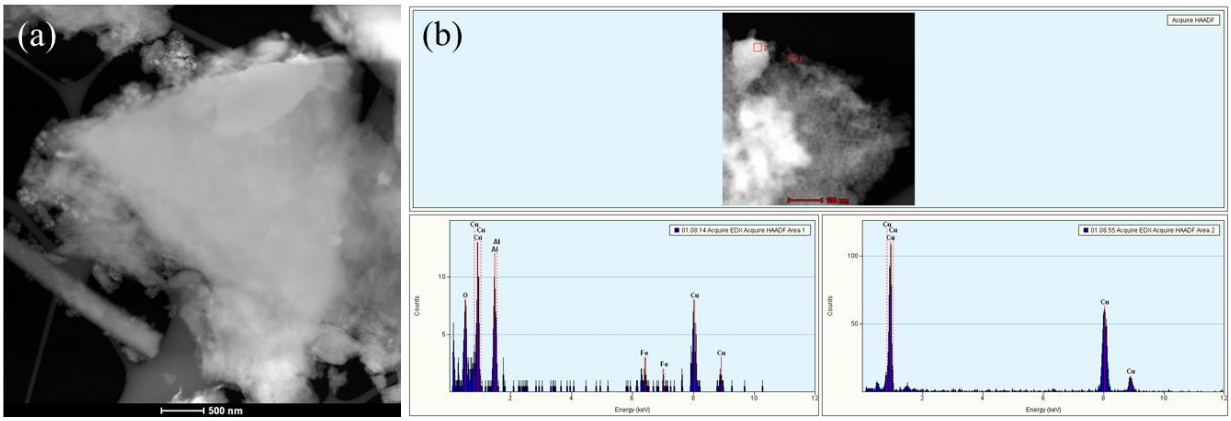

Figure S12. (a) STEM image and (b) EDX of used CFNP09. The bright white areas represent Cu and the lighter gray area represent a mix of CuFe.

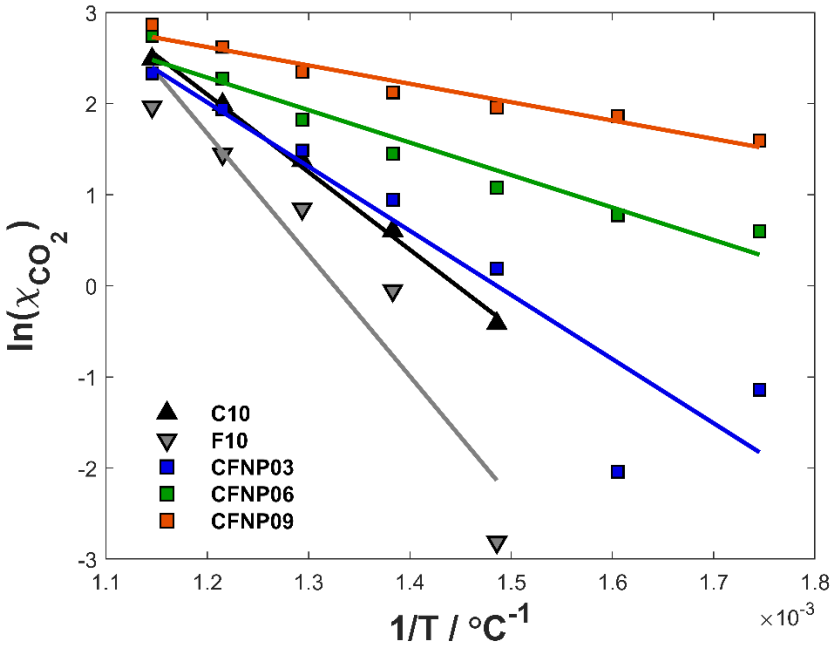

Figure S13: Arrhenius plot of single metal and FeO_x NP doped catalysts. The apparent activation energy of the catalyst drops by increasing the loading of Fe.

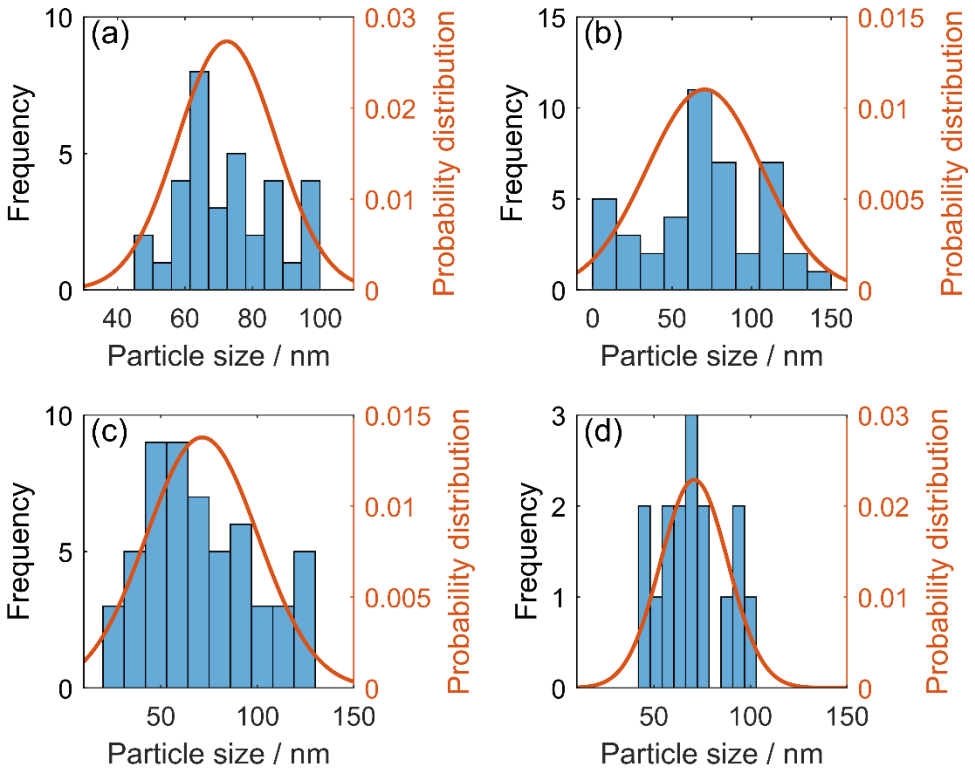

Figure S14:Frequency and probability distribution of the Cu particles on the catalytic surface. (a) CF03, (b) CFNP03, (c) CF09, (d) CFNP09. The particle size is approximately the same confirming that the addition of Fe did not have major effects on the Cu particles previously deposited on the support. It was observed that Cu tended to form agglomerations on the Al_2O_3 surface.

References

(1) Chen, C. S.; Cheng, W. H.; Lin, S. S. Enhanced Activity and Stability of a Cu/SiO2 Catalyst for the Reverse Water Gas Shift Reaction by an Iron Promoter. *Chem. Commun.* **2001**, No. 18, 1770–1771. https://doi.org/10.1039/b104279n.

(2) Pastor-Pérez, L.; Baibars, F.; Le Sache, E.; Arellano-García, H.; Gu, S.; Reina, T. R. CO2 Valorisation via Reverse Water-Gas Shift Reaction Using Advanced Cs Doped Fe-Cu/Al2O3 Catalysts. *J. CO2 Util.* **2017**, *21* (August), 423–428. https://doi.org/10.1016/j.jcou.2017.08.009.

(3) Lin, L.; Yao, S.; Rui, N.; Han, L.; Zhang, F.; Gerlak, C. A.; Liu, Z.; Cen, J.; Song, L.; Senanayake, S. D.; Xin, H. L.; Chen, J. G.; Rodriguez, J. A. Conversion of CO2 on a Highly Active and Stable Cu/FeO:X/CeO2 Catalyst: Tuning Catalytic Performance by Oxide-Oxide Interactions. *Catal. Sci. Technol.* **2019**, *9* (14), 3735–3742. https://doi.org/10.1039/c9cy00722a.

(4) Zhao, K.; Bkour, Q.; Hou, X.; Kang, S. W.; Park, J. C.; Norton, M. G.; Yang, J. Il; Ha, S. Reverse Water Gas Shift Reaction over CuFe/Al2O3 Catalyst in Solid Oxide Electrolysis Cell. *Chem. Eng. J.* **2018**, *336* (August 2017), 20–27. https://doi.org/10.1016/j.cej.2017.11.028.

(5) Yang, L.; Pastor-Pérez, L.; Villora-Pico, J. J.; Sepúlveda-Escribano, A.; Tian, F.; Zhu, M.; Han, Y.-F.; Ramirez Reina, T. Highly Active and Selective Multicomponent Fe–Cu/CeO2–Al2O3 Catalysts for CO2 Upgrading via RWGS: Impact of Fe/Cu Ratio. *ACS Sustain. Chem. Eng.* **2021**,

12155–12166. https://doi.org/10.1021/acssuschemeng.1c03551.

(6) Chen, L.; Wu, D.; Wang, C.; Ji, M.; Wu, Z. Study on Cu-Fe/CeO2 Bimetallic Catalyst for Reverse Water Gas Shift Reaction. *J. Environ. Chem. Eng.* **2021**, *9* (3), 105183. https://doi.org/10.1016/j.jece.2021.105183.

(7) González-Castano, M.; Navarro De Miguel, J. C.; Sinha, F.; Ghomsi Wabo, S.; Klepel, O.; Arellano-Garcia, H. Cu Supported Fe-SiO2 Nanocomposites for Reverse Water Gas Shift Reaction. *J. CO2 Util.* **2021**, *46*, 101493. https://doi.org/10.1016/J.JCOU.2021.101493.

(8) Kunze, J.; Maurice, V.; Klein, L. H.; Strehblow, H. H.; Marcus, P. In Situ STM Study of the Duplex Passive Films Formed on Cu(111) and Cu(001) in 0.1 M NaOH. *Corros. Sci.* **2004**, *46* (1), 245–264. https://doi.org/10.1016/S0010-938X(03)00140-9.

(9) Du, G. H.; Van Tendeloo, G. Cu(OH)2 Nanowires, CuO Nanowires and CuO Nanobelts. *Chem. Phys. Lett.* **2004**, *393* (1–3), 64–69. https://doi.org/10.1016/j.cplett.2004.06.017.

(10) Dahmen, U.; Westmacott, K. H. Ledge Structure and the Mechanism of Θ′ Precipitate Growth in Al-Cu. *Phys. status solidi* **1983**, *80* (1), 249–262. https://doi.org/10.1002/PSSA.2210800128.

(11) Liu, J.; Zhang, A.; Jiang, X.; Liu, M.; Sun, Y.; Song, C.; Guo, X. Selective CO2Hydrogenation to Hydrocarbons on Cu-Promoted Fe-Based Catalysts: Dependence on Cu-Fe Interaction. *ACS Sustain. Chem. Eng.* **2018**, *6* (8), 10182–10190. https://doi.org/10.1021/acssuschemeng.8b01491.